



A pathway to desired functionalities in vertically aligned nanocomposites and related architectures

Aiping Chen* and Quanxi Jia, Guest Editors

Epitaxial vertically aligned nanocomposites (VANs) and their related architectures have shown many intriguing features that are not available from conventional two-dimensional planar multilayers and heterostructures. The ability to control constituent, interface, microstructure, strain, and defects based on VANs has enabled the multiple degrees of freedom to manipulate the optical, magnetic, electrochemical, electronic, ionic, and superconducting properties for specific applications. This field has rapidly expanded from the interest in oxide:oxide to oxide:metal, metal:nitride and nitride:nitride systems. To achieve unparalleled properties of the materials, three-dimensional super-nanocomposites based on a hybrid of VAN and multilayer architectures have been recently explored as well. The challenges and opportunities of VAN films are also discussed in this article.

Introduction

Over the past two decades, new discoveries and major advances have been made in the synthesis of metal oxide thin films and understanding their physical properties such as magnetism, ferroelectricity, and superconductivity. Interface engineering, strain engineering, and defect engineering have been widely used to manipulate functional properties in oxide heterostructures.^{1,2} To achieve desired properties for specific applications, composite materials have been widely explored. The most commonly investigated composites in film format include multilayers, superlattices, and nanoparticles in matrix.³ For example, the inclusion of BaZrO₃ (BZO) nanoparticles in high-temperature superconducting YBa₂Cu₃O_{7- δ} (YBCO) film matrix could greatly enhance the supercurrent-carrying capability under a magnetic field.⁴⁻⁶ Since room-temperature multiferroic materials are rare, bilayer films composed of ferroelectric and ferromagnetic (or ferrimagnetic) heterostructures have been used to achieve magnetoelectric effects. Challenges to achieve desired properties based on these structures vary for material systems and applications. For strain-controlled properties, film thickness is often limited to thinner than the critical film thickness, which is often a few tens of nanometers. For interface-controlled properties, the epitaxial strain resulted from the substrate could be accomplished only to a certain

degree, depending on the lattice mismatch and the defect landscape during epitaxial growth.

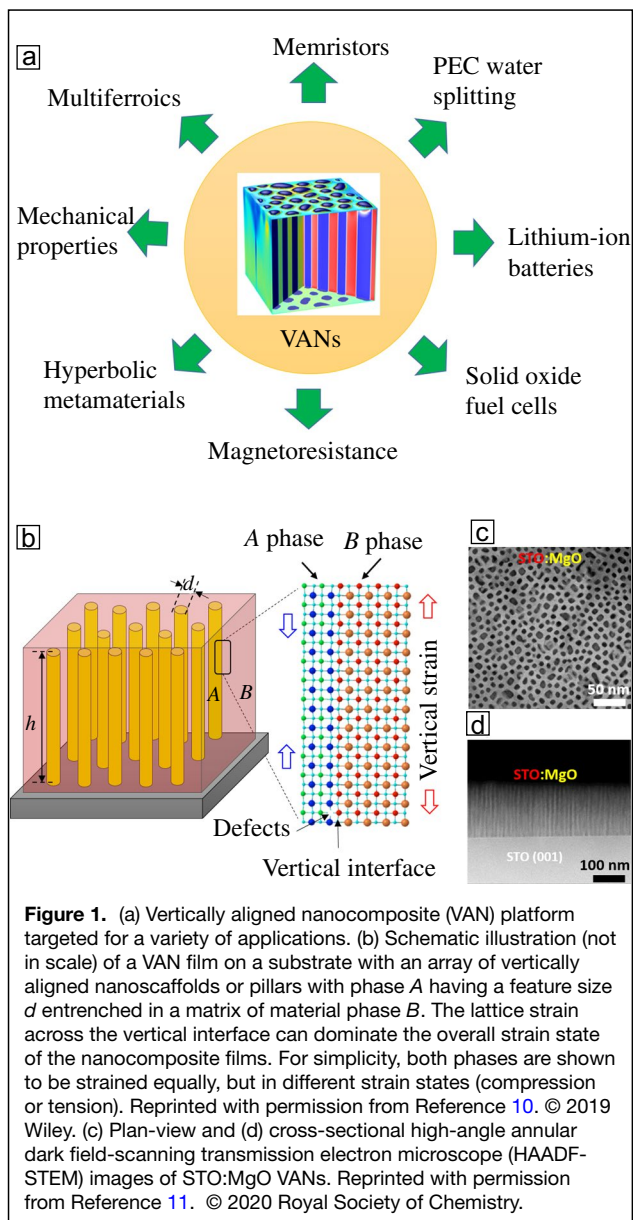
As a unique thin-film architecture, vertically aligned nanocomposites (VANs) have been widely studied in the past decade and great success has been achieved. The VAN thin-film architecture is a unique platform to address some challenging issues in conventional oxide heterostructures.⁷⁻⁹ As discussed later in this article and articles in this issue, VAN has become a powerful architecture to host a variety of functional (e.g., electronic, ionic, dielectric, mechanical, magnetic, superconducting) properties for a range of applications. **Figure 1a** summarizes some applications and functional properties reported in VANs. The enhanced functionalities and emergent behaviors of VAN films can be induced by lattice strain, reduced dimensionality, tunable microstructure (size, distribution, and defects) and coupled vertical interfaces.¹⁰

A wide range of materials systems formed in VAN architecture

VAN is a unique architecture where an array of vertically aligned scaffolds or pillars with nanoscale dimensions are embedded in a film matrix. **Figure 1b** shows a typical illustration of a VAN film with phase *A* as nanopillars and phase *B* as the film matrix. These vertically aligned nanopillars,

Aiping Chen, Center for Integrated Nanotechnologies, Los Alamos National Laboratory, USA; apchen@lanl.gov
Quanxi Jia, Department of Materials Design and Innovation, University at Buffalo, The State University of New York, USA; qxjia@buffalo.edu
*Corresponding author

doi:10.1557/s43577-021-00032-4



with a diameter of d and a length of h , are often formed via self-assembly through the film thickness. Figure 1c–d shows HAADF-STEM images of STO:MgO VANs. The plan-view STEM image shows the MgO pillars (dark contrast) in STO film matrix (gray contrast). The cross-sectional STEM image shows the vertically and alternatively aligned STO and MgO phases.¹¹

To explore the advantages of such an architecture for specific applications, the research community is pursuing two fronts in terms of the selection of materials, *A* and *B*. By choosing materials both *A* and *B* with certain functionalities, one could achieve new and/or emergent properties not from any of the constituents in the nanocomposite if *A* and *B* are coupled across the interface. In oxide:oxide VANs, the most widely investigated

materials are multiferroic $\text{BaTiO}_3:\text{CoFe}_2\text{O}_4$ (BTO:CFO) and $\text{BiFeO}_3:\text{CoFe}_2\text{O}_4$ (BFO:CFO), where BTO (or BFO) and CFO show ferroelectric and ferromagnetic properties, respectively; but magnetoelectricity is accomplished in the BTO:CFO, BFO:CFO and other related VANs.^{7,12–15} In their article in this issue, Gao et al. have discussed the design of strain, interface, and orientation to optimize the magnetoelectric couplings in a variety of ferroelectric:ferromagnetic VANs.¹⁶ In metal:oxide VAN system, noble metal Ir nanopillars embedded in SrTiO_3 (STO) film matrix show intriguing photoelectrochemical (PEC) properties, where the formation of tubular Schottky junctions around each pillar is attributed to the much enhanced photocarrier transport efficiency.¹⁷ In their article in this issue, Lippmaa et al. have described the approaches to design such structures and optimize the water splitting performance.¹⁸ It is noted that similar designs have also been used in oxide:oxide VANs.^{19,20} PEC water-splitting devices with decorated nanowire/nanotube arrays are often fabricated by multiple steps.²¹ In contrast, PEC devices based on VAN structure only require a one-step process. In nitride:nitride VAN systems, where the nitride generally shows excellent wear resistance and metallic properties, early work has studied the spinodal decomposition of $\text{Ti}_{1-x}\text{Al}_x$ films into coherent cubic metastable nanodomains, resulting in an increase in hardness.²²

One could also select material *B* as the matrix (typically ternary metal oxide) with targeted functionality and material *A* as the nanoscaffolds (usually binary metal oxide), where nanoscaffolds or vertically aligned pillars *A* are used to improve or tune the functionalities of matrix *B*. In this case, it is possible to choose a much broader range of materials with targeted electrical, ionic, magnetic, optical, thermal, and/or mechanical properties for specific applications. Examples include $\text{BiFeO}_3:\text{Sm}_2\text{O}_3$, $\text{LSMO}:\text{ZnO}$, and $\text{SrTiO}_3:\text{Sm}_2\text{O}_3$, where the active phases such as BiFeO_3 , LSMO, and SrTiO_3 show ferroelectric, ferromagnetic, and ionic properties, respectively.^{8,23–25} In metal:oxide VAN system, magnetic metal pillars have been studied in oxide film matrix.^{26–28} In their article in this issue, Hennes et al. discuss the magnetic anisotropy and composition modulation in metal:oxide VAN systems.²⁹ The rapid development in this field has been discussed in other reviews.^{10,30–35}

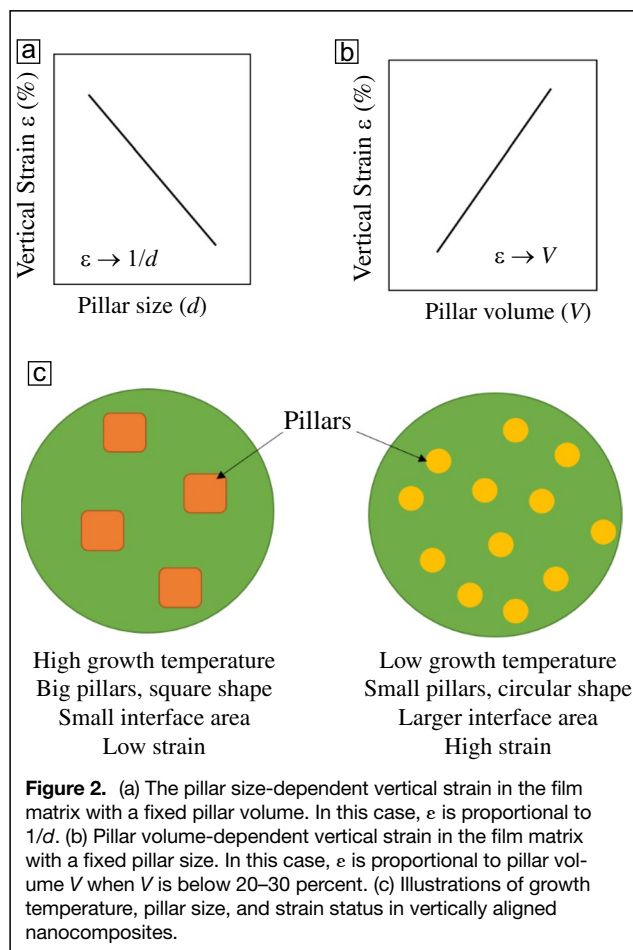
The formation of VAN and the role of pillar size on film morphology

VAN formation can be categorized into two major mechanisms: (1) diffusion, nucleation, and growth for materials systems with limited miscibility; and (2) spinodal decomposition or pseudospinodal decomposition for materials systems with miscibility. For many systems previously discussed, they belong to the first scenario. In alloy compounds such as $\text{Zn}(\text{Ga}, \text{Mn})_2\text{O}_4$, and $\text{Al}_{1-x}\text{Zr}_x\text{N}$, VAN can be formed via pseudospinodal decomposition.³⁶

The final microstructure (pillar size, shape, and lateral spacing) of a VAN is determined by the minimization of the total free energy which includes the elastic and interfacial

energies of the system (two phases and the substrate) at a given growth condition.¹⁰ Phase-field simulation has been able to simulate a variety of different VAN structures. It shows that the final equilibrium structure is determined by the thermodynamic parameters—elastic and interface energies and fractions of the phases.³⁷ In pulsed laser deposition (PLD), a popular method to grow these VANs, growth kinetics such as laser energy density can also play a critical role in determining the final microstructure of the films.

Pillar size is one of the most fundamental parameters in VANs as it determines many other critical parameters such as interfacial area/density, strain state, and defect density.¹⁰ It has been reported that vertical strain (ϵ) is inversely proportional to pillar size d in Ni:STO VANs with a fixed Ni volume,³⁸ as shown in Figure 2a. Figure 2b shows that vertical strain is proportional to the total volume of the secondary phase with a fixed pillar size.³⁹ These results are consistent since pillar size and volume predominantly determine the interfacial area at the vertical interface. Assuming the pillar arrays with m pillars, a feature size of d , a height of h and a total volume of V , as shown in Figure 1. $V = \pi(d/2)^2mh$ and $S = \pi dmh$. Therefore, the total interfacial area $S = 4V/d$. According to the results shown in Figure 2a–b, the vertical strain is proportional to the total interfacial area.³⁹ Figure 2c



shows the general correlation among growth temperature, pillar size, and strain state. In a system with a fixed secondary phase volume, a higher growth temperature will generally produce larger pillar size. This will result in a smaller interfacial area, which usually leads to a lower vertical strain. On the other hand, a lower growth temperature generally results in a smaller pillar size and larger interface area, which can lead to a larger vertical strain. In a system with fixed pillar size, the increase of the pillar density can increase the total vertical interface area and thus lead to a larger strain.

The morphology of the nanopillars appears mostly in circular and/or square. The size of the pillars varies from a few nanometers to more than 100 nm. One of the critical questions will be what factors determine the pillar size and shape? Since the formation of self-assembled VAN structure is closely related to the surface diffusion, material diffusion coefficient and temperature are the most important factors in controlling the lateral size of pillars. For example, oxides such as MgO with low surface diffusion rate often show a pillar size of 5–10 nm at a growth temperature of 700°C.¹¹ On the other hand, the pillar size of BFO can be as large as 50–100 nm at a growth temperature around 700°C, due to the much higher surface diffusion rate of BFO. Using growth temperature to control the pillar size in a VAN film has been widely reported in the literature.

The surface morphology of the pillars is often entangled with their feature size.²⁸ For a given material system, pillars with smaller size, in general, tend to show circular shape while pillars with bigger size tend to show square/rectangle shape as shown in Figure 2c. This is because that the competition between the surface energy and the elastic energy of the phase A (pillar) interacted with the phase B (film matrix) plays a critical role in pillar formation. There is a critical length r_0 ($r_0 = \sigma/4E^*$, σ is the surface energy and E^* is proportional to ϵ^2 and ϵ is the out-of-plane strain in the pillar phase), which represents the relative contribution of the surface and elastic effects.⁴⁰ The relative energy of the pillar phase is determined by its shape and its size relative to the dimensionless critical length, r_0 . The transition from circular shape to square shape occurs around $d = 4r_0$. Larger strain ϵ often corresponds to smaller pillar size, which is consistent with Figure 2c. In addition, the size and pillar distribution strongly impact the strain distribution. Farmer et al. reported the observation of a radial dependence in the magnetic anisotropy of epitaxially strained CFO nanopillars in a BTO matrix. They attributed the out-of-plane uniaxial magnetic anisotropy to the large magnetostriction of CFO and the state of stress within the nanocomposite.⁴¹ The microscopic mechanisms of the correlation between such behavior and the strain/stoichiometry/microstructure/defect have rarely been explored in nanoscale.

Apart from regular pillar structures, interesting lamellar structure has often been observed in systems with two different symmetries such as cubic and hexagonal. For example, it was reported that the formation of a lamellar structure by cubic ZrN and hexagonal AlN phases during the growth of

Zr_{0.69}Al_{0.31}N films by decomposition.⁴² Similar behavior has also been reported in VANs with pseudo-cubic LSMO and hexagonal ZnO phases on cubic substrates.^{43,44}

Unique features and tunable functionalities

Given the distinctive architectures, VANs provide some unique features (not available from conventional heterostructures) that can be explored to tune the functional properties.⁴⁵ Many interesting features from a specific VAN system are closely related to the pillar size and the pillar distribution.¹⁰

Vertical interface strain can dominate the overall strain state in VANs. Experimental results have shown that the strain is ultimately controlled by the vertical interfacial area and the coherence of the vertical interface.³⁹ Similar to heteroepitaxial strain induced by substrate, vertical strain in VANs plays a critical role in tuning functional properties.⁴⁶ As discussed by MacManus-Driscoll and co-workers, the vertical strain, induced by the vertical lattice coupling, goes beyond the conventional critical thickness limitation. In other words, lattice strain can exist in much thicker films.^{39,47} Strain tuned functional properties in many complex metal oxides have been investigated in VANs. For instance, vertical interface strain in VANs has been used to tune the magnetoresistance,³⁹ the magnetic anisotropy,^{12,48,49} and the superconductivity.⁵⁰ In their article in this issue, Huang et al. summarized the strain controlled functionalities in magnetic and ferroelectric VANs.⁵¹ It is also noted that epitaxial stabilization and strain engineering in heterostructures have often been used to stabilize metastable phases such as HfO₂ and others.⁵² In VANs, the stabilization of new phases has not been extensively investigated.⁵³ However, VAN has been explored to stabilize and enhance ferroelectricity in paraelectric STO and ferroelectric BTO.^{11,47,54}

Vertical interfaces through the film thickness in VANs can be considered as the guided networks to enhance certain properties of the materials. In other words, the vertical interfaces can serve as the predefined channels to achieve desired properties for different applications such as solid oxide fuel cells,^{55,56} memristors,²⁴ PEC water splitting,^{17,19} lithium-ion batteries,⁵⁷ and so on. The nanoionic application of VANs has been previously reviewed.⁵⁸ In their article in this issue, Chunha and Huijben discussed the use of vertical interface in VAN to advance solid-state batteries.²⁹ In addition, defects such as oxygen vacancies generated along the vertical interface have been found to be critical to conduction along the vertical interface.^{59,60} In nitride/nitride systems, VANs with the cubic ZrN phase and the hexagonal AlN phase in a nano-labyrinthine structure exhibit enhanced hardness and fracture resistance compared to single-phase ZrN and AlN.⁴² The collective effects from the hindering of dislocation motion and the lack of common glide planes at the vertical interface are responsible for the enhanced mechanical properties. The interesting microstructures resulted from the vertical interface could also be used to manipulate the magneto-transport properties that has been discussed by Wang in his article in this issue.⁶¹

Strong coupling across the vertical interface in VANs can be used to accomplish emergent and new properties. Multiferroic magnetoelectric system based on VANs is a well-studied example in literature to show such a coupling across vertical interface. In their article in this issue, Gao et al. have discussed the advantages of the VAN structure to tune magnetoelectric couplings between ferroelectric and ferromagnetic components.¹⁶ VAN structure could be potentially used as a platform for vertical *p-n* junction arrays which could be an ideal structure to design optoelectronic devices such as photovoltaic devices and PEC water-splitting cells.

Other interfacial phenomena such as exchange bias,^{62,63} photostriction-magnetostriction coupling,⁶⁴ and magneto-photoluminescent coupling⁶⁵ have also been investigated in VANs with combination of different materials. Recently, Wang et al. have explored a variety of oxide/metal systems such as Au:ZnO VANs and metal/nitride (Ag:TiN, Au:AlN) VANs to tune hyperbolic metamaterial properties and magneto-optical effect.⁶⁶⁻⁶⁹ Such efforts have been summarized in a recent review article.⁶⁶

Processes for the formation of self-assembled VAN structures

VAN films are often grown by PLD as shown in **Figure 3a**, where a composite pellet with two premixed phases (phase *A* plus phase *B*) is used as the target. The volume ratio of these two phases in the target is designed based on specific objectives. It is noted, however, a single-phase target can be used if spinodal decomposition controls the growth.^{17,42} Interestingly, VAN structure can be also synthesized by using two separate single-phase targets of phases *A* and *B* as shown in **Figure 3b**. In this case, phases *A* and *B* were deposited sequentially; the volume ratio of these two phases can be tuned by adjusting the pulse number on each target. Compared to the single-target method, one of significant advantages of the multiple target method is that it allows a simple way to tune the composition of VANs. Aimon et al. reported the growth BFO:CFO VANs by alternatively ablating BFO and CFO targets. The process is quite similar to the growth of a multilayer film. However, it was claimed that each “layer” is designed to be less than one unit cell to ensure that continuous single phase film will not be formed.⁷⁰ Liu et al. reported the synthesis of CFO:SRO VANs by using the same dual-target method.⁶⁴ Recently, Tang et al. deposited a multilayer of CuFe₂O₄ (5.2 nm)/BiFeO₃ (7.8 nm) by alternately growth of these two materials at 700°C. Interestingly, VAN films have been obtained after annealing.⁷¹ Therefore, multilayer films can be converted into VANs (**Figure 3b**). In fact, conversion from VAN to multilayers have been seen in the YBCO:BZO system.⁷² However, the mechanisms of the transformation between VAN and multilayer structures, as shown in **Figure 3b**, is still largely unknown. In the oxide/metal system, Bonilla et al. reported the formation of VANs with Co_xNi_{1-x} nanowires in a CeO₂ film matrix by sequentially ablating Co, Ni, and CeO₂ targets, as shown in

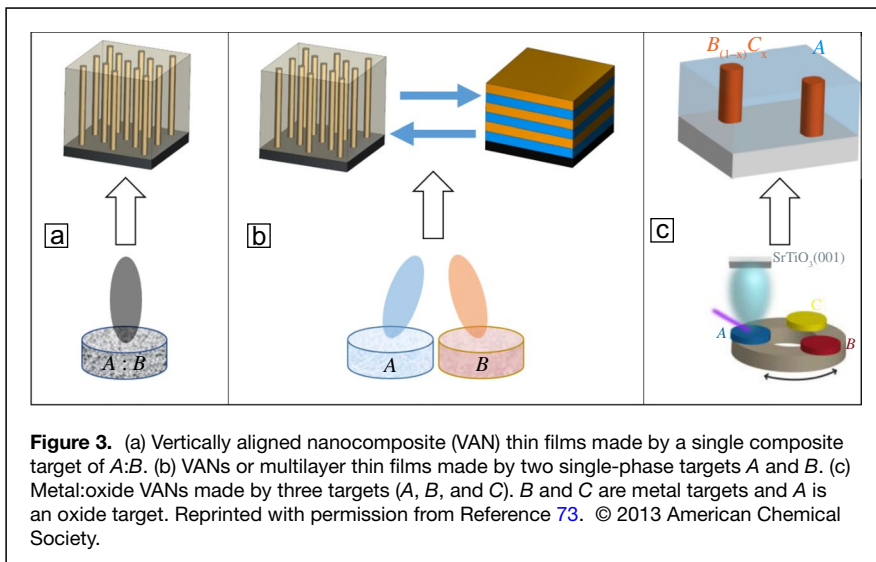


Figure 3c.⁷³ In this issue, Hennes et al. have discussed such a method to generate more advanced nanostructures.⁷⁴ In the deposition setup configuration described in Figure 3b and c, targets can be rotated but the substrate location is fixed.

The dual-target method and the sequential growth, combined with moving the substrate correspondingly, can be effectively used for the combinatorial thin-film growth.⁷⁵ For example, combinatorial (C)PLD has been often used to make composition spread for oxide thin films. Ross and co-workers have used this method to synthesize a variety of oxide nanocomposites.^{65,76,77}

Formation of 3D supernanocomposites

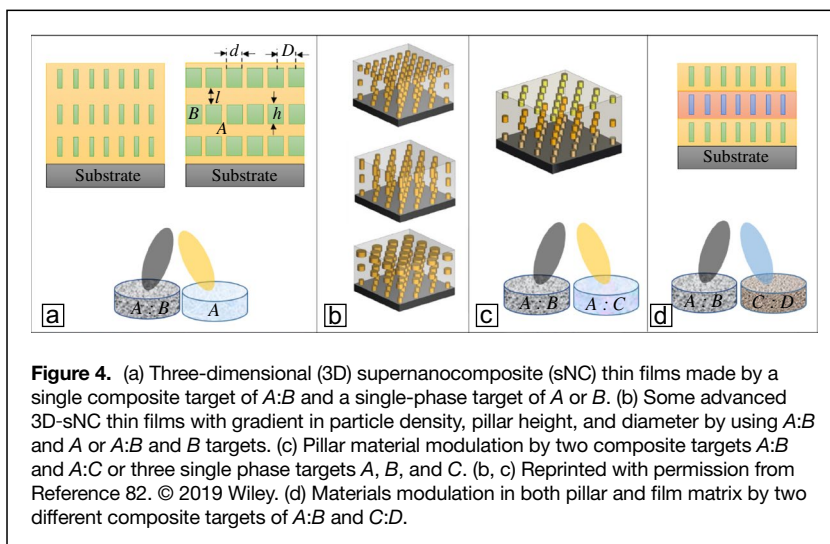
As previously discussed, VAN is an appealing platform to host different types of materials, including oxide:oxide, oxide:metal, metal:nitride and nitride:nitride systems to achieve desired functional and structural properties. To further push the envelope of the synthesis and materials design, one can envision that unprecedented opportunities exist if a 3D architecture is constructed by integrating superlattice and VAN structures. Recently, advances in 3D supernanocomposites (3D-sNCs) have been demonstrated to take the full advantage of multilayers or superlattices and the VANs.

In the configuration of two targets as shown in Figure 4a, one of the targets is a composite target such as $A:B$ and the other one is A or B . Some interesting new structures have been reported based on such ideas. Kim et al. reported the growth of spinel

bilayer pillars in BFO film matrix via a CPLD method.⁷⁷ Ning et al. have fabricated NiO short nanopillar arrays in a LSMO film matrix.⁷⁸ Sun et al. explored the configurations of LSMO: CeO_2 /LSMO ($A:B/A$) and LSMO: CeO_2 / CeO_2 ($A:B/B$).⁷⁹ In addition, a nanodumbbell structure was generated by using two LSMO: CeO_2 composite targets with different CeO_2 doping levels.⁸⁰ A simple change in target configuration has produced a variety of nanostructures with interesting microstructures. These microstructures play important roles in functional properties. Li et al. fabricated BFO nanoparticle arrays in a CFO film matrix to reduce the leakage current in magnetoelectric VANs.⁸¹ In the article in

this issue, Wang discusses the microstructure design in such 3D-sNCs to tune magnetoresistance properties.⁶¹

Furthermore, one of the key advantages of such an architecture is that it can be utilized to fabricate nanocomposites (nanoparticles in film matrix structure) with good controllability in terms of the feature size and distribution of the nanostructured phase through the film thickness. Conventional architectures of making such nanostructures have the challenges such as the random distribution of particles in size and density, and particle aggregation. By combining the multilayer and VAN growth, Figure 4b shows the 3D-sNCs that offer the ability to control the particle size (d), height (h), vertical spacing (l), and lateral spacing (D).⁸² Therefore, the composition and distribution of nanoparticles can be controlled in such 3D-sNCs. In fact, with the ability of controlling various density, height, and feature



size of nanoparticles, these structures can be used as the basic building blocks to design more complex nanostructures. Figure 4b shows some possible combinations. For example, such a design permits the synthesis of 3D-sNCs with modulated particle density by changing the composition of the cylinders in the VAN layers, the nanocylinder height by varying the VAN layer thickness, or the nanocylinder feature size by changing the substrate temperature. It also allows the design of targeted chemistry by changing the nanocylinder material in the VAN layers (Figure 4c) as well as the film matrix in each layer (Figure 4d). Such a structure (Figure 4c) has been realized in the MgFe₂O₄:BFO/BFO/CFO:BFO system.⁷⁷ A similar structure of Au:BTO/ZnO:BTO have also been realized to explore the optical properties.⁸³ These different structures shown in Figure 4 can be engineered together to produce even more complex nanostructures. Importantly, this design strategy allows for the unprecedented control of complex nanocomposites with detailed manipulation of the nanocylinder size, spacing, and distribution at the nanoscale.

Conclusions and future opportunities

Thanks to the dedication from researchers worldwide, a variety of epitaxial VANs have been successfully synthesized and studied over the past decade. VAN has become a unique platform to host different types of material systems such as oxide:oxide, oxide:metal, metal:nitride and nitride:nitride for achieving various functional and mechanical properties. Our understanding on the synthesis and growth–microstructure–property correlation of VAN has evolved significantly. Efforts in phase-field simulation have helped to understand the formation process and some interfacial coupling properties of VANs. Rapid developments in advanced characterization techniques at nanoscale are critical to probe the microstructure, interface, strain, and defects in VANs and to establish the microstructure–strain–defect correlation.

Even so, much efforts are needed to address the challenges related to the synthesis and characterization of nanocomposites with desired properties. First, the exploration of the VANs formation process by *in situ* and *ex situ* diagnose techniques could be extremely useful to better understand the synthesis–defect–strain–interface–function correlation. Second, the deconvolution of the roles of defect, interface, strain, interface coupling, and microstructure on the physical properties of the VANs requires fully integrated efforts from controlled synthesis, advanced characterization, and modeling/simulation. Third, developing VAN related 3D-sNCs with even more complex chemical compositions is still in its early stage. We expect that 3D-sNC structure could open new avenues to fabricate advanced nanostructures, which are not feasible from conventional architectures. We hope this issue in VANs will inspire researchers worldwide to leverage the advantages of VAN and VAN-related structures and compositions to address the scientific and technological challenges in their fields.

Acknowledgments

The work at Los Alamos National Laboratory was supported by the NNSA's Laboratory Directed Research and Development Program and was performed, in part, at the Center for Integrated Nanotechnologies (CINT), an Office of Science User Facility operated for the US Department of Energy Office of Science. Los Alamos National Laboratory, an affirmative action equal opportunity employer, is managed by Triad National Security, LLC for the US Department of Energy's NNSA, under contract 89233218CNA000001. The effort at University at Buffalo was supported by the US National Science Foundation, ECCS-1902623. Q.X. J. acknowledges support from the CINT Users Program.

Conflict of interest

The authors declare that there is no conflict of interest.

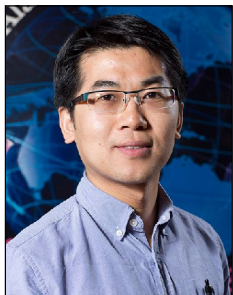
Open Access

This article is licensed under a Creative Commons Attribution 4.0 International License, which permits use, sharing, adaptation, distribution and reproduction in any medium or format, as long as you give appropriate credit to the original author(s) and the source, provide a link to the Creative Commons license, and indicate if changes were made. The images or other third party material in this article are included in the article's Creative Commons license, unless indicated otherwise in a credit line to the material. If material is not included in the article's Creative Commons license and your intended use is not permitted by statutory regulation or exceeds the permitted use, you will need to obtain permission directly from the copyright holder. To view a copy of this license, visit <http://creativecommons.org/licenses/by/4.0>.

References

1. H.Y. Hwang, Y. Iwasa, M. Kawasaki, B. Keimer, N. Nagaosa, Y. Tokura, *Nat. Mater.* **11**, 103 (2012)
2. J.R. Petrie, C. Mitra, H. Jeon, W.S. Choi, T.L. Meyer, F.A. Reboredo, J.W. Freeland, G. Eres, H.N. Lee, *Adv. Funct. Mater.* **26**, 1564 (2016)
3. H. Guo, Z. Wang, S. Dong, S. Ghosh, M. Saghayezhian, L. Chen, Y. Weng, A. Herklotz, T.Z. Ward, R. Jin, S.T. Pantelides, Y. Zhu, J. Zhang, E.W. Plummer, *Proc. Natl. Acad. Sci. U.S.A.* **114**, E5062 (2017)
4. T. Haugan, P.N. Barnes, R. Wheeler, F. Meisenkothen, M. Sumption, *Nature* **430**, 867 (2004)
5. A. Llordes, A. Palau, J. Gazquez, M. Coll, R. Vlad, A. Pomar, J. Arbiol, R. Guzman, S. Ye, V. Rouco, F. Sandiumenge, S. Ricart, T. Puig, M. Varela, D. Chateigner, J. Vanacken, J. Gutierrez, V. Moshchalkov, G. Deutscher, C. Magen, X. Obradors, *Nat. Mater.* **11**, 329 (2012)
6. J.L. MacManus-Driscoll, S.R. Foltyn, Q.X. Jia, H. Wang, A. Serquis, L. Civale, B. Maiorov, M.E. Hawley, M.P. Maley, D.E. Peterson, *Nat. Mater.* **3**, 439 (2004)
7. H. Zheng, J. Wang, S.E. Lofland, Z. Ma, L. Mohaddes-Ardabili, T. Zhao, L. Salamanca-Riba, S.R. Shinde, S.B. Ogale, F. Bai, D. Viehland, Y. Jia, D.G. Schlom, M. Wuttig, A. Roytburd, R. Ramesh, *Science* **303**, 661 (2004)
8. J.L. MacManus-Driscoll, P. Zerrer, H.Y. Wang, H. Yang, J. Yoon, A. Fouchet, R. Yu, M.G. Blamire, Q.X. Jia, *Nat. Mater.* **7**, 314 (2008)
9. J.L. MacManus-Driscoll, A. Suwardi, H. Wang, *MRS Bull.* **40**, 933 (2015)
10. A.P. Chen, Q. Su, H. Han, E. Enriquez, Q.X. Jia, *Adv. Mater.* **31**, 1803241 (2019)
11. E. Enriquez, Q. Li, P. Bowlan, P. Lu, B. Zhang, L. Li, H. Wang, A.J. Taylor, D. Yarotski, R.P. Prasankumar, S.V. Kalinin, Q.X. Jia, A.P. Chen, *Nanoscale* **12**, 18193 (2020)
12. N. Dix, R. Muralidharan, J.M. Rebled, S. Estrade, F. Peiro, M. Varela, J. Fontcuberta, F. Sanchez, *ACS Nano* **4**, 4955 (2010)

13. A.P. Chen, Y. Dai, A. Eshghinejad, Z. Liu, Z. Wang, J. Bowlan, E. Knall, L. Civale, J.L. MacManus-Driscoll, A.J. Taylor, R.P. Prasadkumar, T. Lookman, J. Li, D. Yarotski, Q.X. Jia, *Adv. Sci.* **6**, 1901000 (2019)
14. Y.S. Oh, S. Crane, H. Zheng, Y.H. Chu, R. Ramesh, K.H. Kim, *Appl. Phys. Lett.* **97**, 052902 (2010)
15. G. Dong, Z. Zhou, M. Guan, X. Xue, M. Chen, J. Ma, Z. Hu, W. Ren, Z.-G. Ye, C.-W. Nan, *ACS Nano* **12**, 3751 (2018)
16. M. Gao, Y. Yang, W.-F. Rao, D. Viehland, *MRS Bull.* **46** (2), 123 (2021)
17. S. Kawasaki, R. Takahashi, T. Yamamoto, M. Kobayashi, H. Kumigashira, J. Yoshinobu, F. Komori, A. Kudo, M. Lippmaa, *Nat. Commun.* **7**, 11818 (2016)
18. M. Lippmaa, S. Kawasaki, R. Takahashi, T. Yamamoto, *MRS Bull.* **46** (2), 142 (2021)
19. T.H. Do, C. Nguyen Van, K.-A. Tsai, L.T. Quynh, J.-W. Chen, Y.-C. Lin, Y.-C. Chen, W.-C. Chou, C.-L. Wu, Y.-J. Hsu, Y.-H. Chu, *Nano Energy* **23**, 153 (2016)
20. L.T. Quynh, C.N. Van, Y. Bitla, J.W. Chen, T.H. Do, W.Y. Tzeng, S.C. Liao, K.A. Tsai, Y.C. Chen, C.L. Wu, C.H. Lai, C.W. Luo, Y.J. Hsu, Y.H. Chu, *Adv. Energy Mater.* **6**, 1600686 (2016)
21. H. Han, F. Karlicky, S. Pitchaimuthu, S.H.R. Shin, A.P. Chen, *Small* **15**, 1902771 (2019)
22. P.H. Mayrhofer, A. Hörling, L. Karlsson, J. Sjöln, L. Larsson, C. Mitterer, L. Hultman, *Appl. Phys. Lett.* **83**, 2049 (2003)
23. A.P. Chen, Z.X. Bi, C.F. Tsai, J. Lee, Q. Su, X.H. Zhang, Q.X. Jia, J.L. MacManus-Driscoll, H.Y. Wang, *Adv. Funct. Mater.* **21**, 2423 (2011)
24. S. Lee, A. Sangle, P. Lu, A.P. Chen, W.R. Zhang, J.S. Lee, H.Y. Wang, Q.X. Jia, J.L. MacManus-Driscoll, *Adv. Mater.* **26**, 6284 (2014)
25. H. Yang, H.Y. Wang, J. Yoon, Y.Q. Wang, M. Jain, D.M. Feldmann, P.C. Dowden, J.L. MacManus-Driscoll, Q.X. Jia, *Adv. Mater.* **21**, 3969 (2009)
26. Q. Su, W.R. Zhang, P. Lu, S.M. Fang, F. Khatkhatay, J. Jian, L.G. Li, F.L. Chen, X.H. Zhang, J.L. MacManus-Driscoll, A.P. Chen, Q.X. Jia, H.Y. Wang, *ACS Appl. Mater. Interfaces* **8**, 20283 (2016)
27. Y. Roussigne, S.M. Cherif, A.A. Stashkevich, F. Vidal, Y. Zheng, *J. Appl. Phys.* **118**, 233903 (2015)
28. L. Mohaddes-Ardabili, H. Zheng, Q. Zhan, S.Y. Yang, R. Ramesh, L. Salamanca-Riba, M. Wuttig, S.B. Ogale, X. Pan, *Appl. Phys. Lett.* **87**, 203110 (2005)
29. D.M. Cunha, M. Huijben, *MRS Bull.* **46** (2), 152 (2021)
30. J.L. MacManus-Driscoll, *Adv. Funct. Mater.* **20**, 2035 (2010)
31. A.P. Chen, Z.X. Bi, Q.X. Jia, J.L. MacManus-Driscoll, H.Y. Wang, *Acta Mater.* **61**, 2783 (2013)
32. W.R. Zhang, A.P. Chen, Z.K. Bi, Q.X. Jia, J.L. MacManus-Driscoll, H.Y. Wang, *Curr. Opin. Solid State Mater. Sci.* **18**, 6 (2014)
33. W.R. Zhang, R. Ramesh, J.L. MacManus-Driscoll, H.Y. Wang, *MRS Bull.* **40**, 736 (2015)
34. J. Huang, J.L. MacManus-Driscoll, H. Wang, *J. Mater. Res.* **32**, 4054 (2017)
35. X. Sun, J.L. MacManus-Driscoll, H. Wang, *Annu. Rev. Mater. Res.* **50**, 229 (2019)
36. S. Park, Y. Horibe, T. Asada, L.S. Wielunski, N. Lee, P.L. Bonanno, S.M. O'Malley, A.A. Sirenko, A. Kazimirov, M. Tanimura, T. Gustafsson, S.W. Cheong, *Nano Lett.* **8**, 720 (2008)
37. A. Artemev, J. Slutsker, A.L. Roytburd, *Acta Mater.* **53**, 3425 (2005)
38. V. Schuler, F.J. Bonilla, D. Demaille, A. Coati, A. Vlad, Y. Garreau, M. Sauvage-Simkin, A. Novikova, E. Fonda, S. Hidki, V. Etgens, F. Vidal, Y.L. Zheng, *Nano Res.* **8**, 1964 (2015)
39. A.P. Chen, J.-M. Hu, P. Lu, T.N. Yang, W. Zhang, L. Li, T. Ahmed, E. Enriquez, M. Weigand, Q. Su, H.Y. Wang, J.-X. Zhu, J.L. MacManus-Driscoll, L.Q. Chen, D. Yarotski, Q.X. Jia, *Sci. Adv.* **2**, e1600245 (2016)
40. M. McCormack, A. Khachatryan, J. Morris Jr., *Acta Metall. Mater.* **40**, 325 (1992)
41. T.O. Farmer, E.-J. Guo, R.D. Desautels, L. DeBeer-Schmitt, A.P. Chen, Z. Wang, Q.X. Jia, J.A. Borchers, D.A. Gilbert, B. Holladay, S.K. Sinha, M.R. Fitzsimmons, *Phys. Rev. Mater.* **3**, 081401 (2019)
42. N. Ghafoor, I. Petrov, D. Holec, G. Greczynski, J. Palisaitis, P.O. Persson, L. Hultman, J. Birch, *Sci. Rep.* **8**, 1 (2018)
43. A.P. Chen, W.R. Zhang, F. Khatkhatay, Q. Su, C.F. Tsai, L. Chen, Q.X. Jia, J.L. MacManus-Driscoll, H. Wang, *Appl. Phys. Lett.* **102**, 093114 (2013)
44. A.P. Chen, M. Weigand, Z. Bi, W. Zhang, X. Lu, P. Dowden, J.L. MacManus-Driscoll, H. Wang, Q.X. Jia, *Sci. Rep.* **4**, 5426 (2014)
45. H.-J. Liu, W.-I. Liang, Y.-H. Chu, H. Zheng, R. Ramesh, *MRS Commun.* **4**, 31 (2014)
46. J. MacManus-Driscoll, A. Suwardi, A. Kursumovic, Z.X. Bi, C.F. Tsai, H.Y. Wang, Q.X. Jia, O.J. Lee, *APL Mater.* **3**, 062507 (2015)
47. S.A. Harrington, J.Y. Zhai, S. Denev, V. Gopalan, H.Y. Wang, Z.X. Bi, S.A.T. Redfern, S.H. Baek, C.W. Bark, C.B. Eom, Q.X. Jia, M.E. Vickers, J.L. MacManus-Driscoll, *Nat. Nanotechnol.* **6**, 491 (2011)
48. W. Zhang, J. Jian, A.P. Chen, L. Jiao, F. Khatkhatay, L. Li, F. Chu, Q.X. Jia, J.L. MacManus-Driscoll, *Appl. Phys. Lett.* **104**, 062402 (2014)
49. H. Zheng, J. Kreisel, Y.H. Chu, R. Ramesh, L. Salamanca-Riba, *Appl. Phys. Lett.* **90**, 113113 (2007)
50. E.-M. Choi, A. Di Bernardo, B. Zhu, P. Lu, H. Alpner, K.H.L. Zhang, T. Shapira, J. Feighan, X. Sun, J. Robinson, Y. Pattiel, O. Millo, H. Wang, Q.X. Jia, J.L. MacManus-Driscoll, *Sci. Adv.* **5**, eaav5532 (2019)
51. J. Huang, W. Li, H. Yang, J.L. MacManus-Driscoll, *MRS Bull.* **46** (2), 159 (2021)
52. Y. Wei, P. Nukala, M. Salverda, S. Matzen, H.J. Zhao, J. Momand, A.S. Everhardt, G. Agnus, G.R. Blake, P. Lecoeur, *Nat. Mater.* **17**, 1095 (2018)
53. K.T. Kang, B. Zhang, Y. Sharma, B. Paudel, H. Wang, P. Dowden, A.P. Chen, *Appl. Phys. Lett.* **117**, 151601 (2020)
54. A.L. Sangle, O.J. Lee, A. Kursumovic, W. Zhang, A.P. Chen, H. Wang, J.L. MacManus-Driscoll, *Nanoscale* **10**, 3460 (2018)
55. W. Ma, J.J. Kim, N. Tsvetkov, T. Daio, Y. Kuru, Z. Cai, Y. Chen, K. Sasaki, H.L. Tuller, B. Yildiz, *J. Mater. Chem. A* **3**, 207 (2015)
56. Q. Su, D. Yoon, A.P. Chen, F. Khatkhatay, A. Manthiram, H.Y. Wang, *J. Power Sources* **242**, 455 (2013)
57. Z. Qi, J. Tang, S. Misra, C. Fan, P. Lu, J. Jian, Z. He, V.G. Pol, X. Zhang, H. Wang, *Nano Energy* **69**, 104381 (2020)
58. S. Lee, J.L. MacManus-Driscoll, *APL Mater.* **5**, 072907 (2017)
59. W.W. Li, R. Zhao, R.J. Tang, A.P. Chen, W.R. Zhang, X. Lu, H.Y. Wang, H. Yang, *ACS Appl. Mater. Interfaces* **6**, 5356 (2014)
60. W.W. Li, W. Zhang, L. Wang, J.X. Gu, A.P. Chen, R. Zhao, Y. Liang, H.Z. Guo, R.J. Tang, C.C. Wang, K.J. Jin, H.Y. Wang, H. Yang, *Sci. Rep.* **5**, 11335 (2015)
61. Z.J. Wang, *MRS Bull.* **46** (2), 131 (2021)
62. W. Zhang, A.P. Chen, J. Jian, Y.Y. Zhu, L. Chen, P. Lu, Q.X. Jia, J.L. MacManus-Driscoll, X.H. Zhang, H.Y. Wang, *Nanoscale* **7**, 13808 (2015)
63. W.R. Zhang, L.G. Li, P. Lu, M. Fan, Q. Su, F. Khatkhatay, A.P. Chen, Q.X. Jia, X.H. Zhang, J.L. MacManus-Driscoll, H.Y. Wang, *ACS Appl. Mater. Interfaces* **7**, 21646 (2015)
64. H.J. Liu, L.Y. Chen, Q. He, C.W. Liang, Y.Z. Chen, Y.S. Chien, Y.H. Hsieh, S.J. Lin, E. Arenholz, C.W. Luo, Y.L. Chueh, Y.C. Chen, Y.H. Chu, *ACS Nano* **6**, 6952 (2012)
65. C. Zhang, D.H. Kim, X. Huang, X.Y. Sun, N.M. Aimon, S.J. Chua, C.A. Ross, *ACS Appl. Mater. Interfaces* **9**, 32359 (2017)
66. X. Wang, H. Wang, *Nanoscale* **12**, 20564 (2020)
67. R.L. Paldi, X. Sun, X. Wang, X. Zhang, H. Wang, *ACS Omega* **5**, 2234 (2020)
68. X. Wang, T. Nguyen, Y. Cao, J. Jian, O. Malis, H. Wang, *Appl. Phys. Lett.* **114**, 023103 (2019)
69. X. Wang, J. Jian, Z. Zhou, C. Fan, Y. Dai, L. Li, J. Huang, J. Sun, A. Donohue, P. Bernel, *Adv. Opt. Mater.* **7**, 1801180 (2019)
70. N.M. Aimon, D.H. Kim, H.K. Choi, C.A. Ross, *Appl. Phys. Lett.* **100**, 092901 (2012)
71. X. Tang, C.M. Leung, M. Gao, C. Winkler, H. Luo, J. Li, D. Viehland, *J. Am. Ceram. Soc.* **102**, 5192 (2019)
72. H. Yang, H. Wang, B. Maiorov, J. Lee, D. Talbayev, M.J. Hinton, D.M. Feldmann, J.L. MacManus-Driscoll, A.J. Taylor, L. Civale, T.R. Lemberger, Q.X. Jia, *J. Appl. Phys.* **106**, 093914 (2009)
73. F.J. Bonilla, A. Novikova, F. Vidal, Y.L. Zheng, E. Fonda, D. Demaille, V. Schuler, A. Coati, A. Vlad, Y. Garreau, M.S. Simkin, Y. Dumont, S. Hidki, V. Etgens, *ACS Nano* **7**, 4022 (2013)
74. M. Hennes, D. Demaille, G. Patriarche, T. Tran, Y. Zheng, F. Vidal, *MRS Bull.* **46** (2), 136 (2021)
75. J. Wang, Y. Yoo, C. Gao, I. Takeuchi, X. Sun, H. Chang, X.-D. Xiang, P.G. Schultz, *Science* **279**, 1712 (1998)
76. D.H. Kim, N.M. Aimon, C.A. Ross, *J. Appl. Phys.* **113**, 17B510 (2013)
77. D.H. Kim, N.M. Aimon, X. Sun, C.A. Ross, *Adv. Funct. Mater.* **24**, 2334 (2014)
78. X.K. Ning, Z.J. Wang, Z.D. Zhang, *Adv. Funct. Mater.* **24**, 5393 (2014)
79. X. Sun, J. Huang, J. Jian, M. Fan, H. Wang, Q. Li, J.L. MacManus-Driscoll, P. Lu, X. Zhang, H. Wang, *Mater. Horiz.* **5**, 536 (2018)
80. X. Sun, Q. Li, J. Huang, M. Fan, B.X. Rutherford, R.L. Paldi, J. Jian, X. Zhang, H. Wang, *Appl. Mater. Today* **16**, 204 (2019)
81. Y.X. Li, Z.C. Wang, J.J. Yao, T.N. Yang, Z.G. Wang, J.M. Hu, C.L. Chen, R. Sun, Z.P. Tian, J.F. Li, L.Q. Chen, D. Viehland, *Nat. Commun.* **6**, 6680 (2015)
82. A.P. Chen, Z. Harrell, P. Lu, E. Enriquez, L. Li, B. Zhang, P. Dowden, C. Chen, H. Wang, J.L. MacManus-Driscoll, Q.X. Jia, *Adv. Funct. Mater.* **29**, 1900442 (2019)
83. S. Misra, D. Zhang, Z. Qi, D. Li, J. Lu, H.-T. Chen, H. Wang, *Cryst. Growth Des.* **20**, 6101 (2020) □



Aiping Chen is a staff scientist at the Center for Integrated Nanotechnologies (CINT) at Los Alamos National Laboratory (LANL). CINT is a US Department of Energy funded user facility, which serves national and international users. After receiving his PhD degree in 2013 from Texas A&M University, he continued research on complex oxides as a director's postdoctoral fellow at LANL. Since 2017, he is leading the efforts on synthesis and characterization of complex oxide heterostructures and nanocomposites at CINT. His recent research focuses on thin-film synthesis, emergent phenomena in quantum materials and electronic devices.

Chen can be reached by email at apchen@lanl.gov.



Quanxi Jia is an Empire Innovation Professor and National Grid Professor of Materials Research at the University at Buffalo (UB), The State University of New York. He is also the scientific director of the New York State Center for Excellence in Materials Informatics. Prior to joining UB in 2016, he was the director of the Center for Integrated Nanotechnologies (CINT), a US Department of Energy Nanoscale Science Research Center operated jointly by Los Alamos and Sandia National Laboratories. His research includes the synthesis and study of processing-structure-property relationships of nanostructured materials, multifunctional materials, and

thin films, as well as the development of microelectronic/electro-optic devices. Jia can be reached by email at qxjia@buffalo.edu.